# Toward Ultracompact Multi-Materials Rectangular Waveguide Terminations

Gautier Zinkiewicz, Alexis Chevalier, Paul Laurent, J. Benedicto, *Member, IEEE*, Azar Maalouf, and Vincent Laur, *Senior Member, IEEE*

***Abstract*— A new multi-materials' compact topology, allowed by multi-materials 3-D-printing, is proposed to design microwave terminations in rectangular waveguide technology. The concept is based on a Salisbury-like resonant absorber constituted of a 3-D-printed polylactic acid (PLA) dielectric spacer and a lossy dielectric in the form of a pad whose dimensions allow controlling the frequency of maximum absorption. The flange of the termination is also printed with a lossy dielectric to achieve a compact and low-weight component that can be directly connected to a standard metallic waveguide. The concept has been validated experimentally in K-band (18–26 GHz) and X-band (8–12 GHz) with relative bandwidths (RBWs) around 20% for both frequency bands. These components demonstrate a quite stable temperature behavior. The power-handling capability (PHC) has been investigated through simulations and experiments. It was demonstrated that the maximum power than can support the termination is around 4–5 times lower than a more standard and bulky termination made with the same materials.**

***Index Terms*— Additive manufacturing, electromagnetic (EM) composite materials and measurements, electro-thermal device modeling, microwave absorbers, microwave measurements, passive components, power-handling capability (PHC).**

## I. Introduction

MICROWAVE terminations (or loads) are key devices in many telecommunication systems. In rectangular waveguide technology, these components are constituted of a short-circuited waveguide in which an absorber is placed. The shape of the absorber mainly depends on the bandwidth required for a given application. These components are usually associated with a coupler or a circulator. As an example, in satellite and radar systems, isolators (circulator + termination) are used to protect components that are sensitive to RF power variations and to impedance mismatch such as amplifiers. In this component, the termination allows absorbing the backward wave. Traditional microwave architectures integrated few microwave terminations so that the cost, size, and weight constraints on these components were not crucial for microwave engineers. However, with the emergence of electronically scanned array technologies, several tens of microwave terminations will have to be integrated due to the parallelization of chains in radar or broadcast systems. For some of these applications, the main constraint is no more the return loss level of the termination (that can be in the order of 10 dB) or the bandwidth of absorption but the size, weight, and cost of the component that have to be minimized.

During the last decades, few laboratory studies were conducted to improve the overall performance of microwave loads. In [1], a metamaterial absorber based on an electric-field-coupled resonator was used to design and fabricate an X-band waveguide termination. This topology led to a very thin component but with a too limited bandwidth of 0.75%. High level of return loss over a wide bandwidth was also achieved by the transversal [2] or longitudinal [3] integration of printed circuit board (PCB) passive devices connected to 50-Ω resistors in metallic rectangular waveguides. Such components provide wide band absorptions together with a small thickness but to the detriment of fabrication complexity (mounting of chip resistors, integration in a metal housing, etc.) especially at high frequency. In parallel, the development of additive manufacturing gave rise to new topological innovations or materials integration. In [4], an original lossy gap waveguide structure fabricated by 3-D printing of a polymer that was further electroless plated demonstrated a return loss level higher than 20 dB over Ka-band. However, despite a spiral shape to decrease the size, this component cannot be considered as more compact than traditional absorber-based terminations. Lossy dielectric can also be shaped using 3-D printing technique. Thus, we demonstrated in [5] and [6] that efficient low-cost low-weight X-band microwave terminations that can be directly connected to a standard waveguide can be fabricated by 3-D-printing of carbon-filled polymers. We further investigated the feasibility to decrease the thickness of the component by a discretization of the absorber in the form of blocks with different heights [7]. In simulation, a reduction of 76% compared to a standard pyramidal topology was demonstrated but, experimentally, this reduction was limited to 52% due to dimensional variations and uncontrolled air gaps. More recently, multi-materials 3-D-printing gave rise to new topological possibilities that are investigated in this study.

This article is an expanded version of [8] in which the concept of multi-materials compact terminations was presented. Here, we detail the design methodology as well as the constraints related to the manufacturing process and

Manuscript received 15 March 2022; revised 24 May 2022; accepted 17 June 2022. Date of publication 14 July 2022; date of current version 13 January 2023. This article is an expanded version from the IEEE Radio & Wireless Week, Las Vegas, Nevada USA, 16–19 January 2022. [DOI: 10.1109/RWS53089.2022.9719958] *(Corresponding author: Vincent Laur.)*

The authors are with the Lab-STICC, UMR 6285, CNRS, Brest University, 29238 Brest, France (e-mail: vincent.laur@univ-brest.fr).

Color versions of one or more figures in this article are available at https://doi.org/10.1109/TMTT.2022.3188318.

Digital Object Identifier 10.1109/TMTT.2022.3188318

the properties of the materials used. The automation of the component temperature test bench and the associated results are also detailed. Finally, an extension of the concept to a different frequency band is proposed and the power handling of the components is evaluated through measurements and thermo-electromagnetic (EM) modeling.

In this article, we studied a multi-material topology of termination that can be printed in a single process and directly connected to a standard waveguide after fabrication without requiring an assembly step or a packaging. The aim is to propose a very compact component for low-power applications with moderate bandwidths. At first, the concept of the topology that is based on a Salisbury in free space is explained. Then, the adaptation of the termination to allow its fabrication with a fused deposition modeling (FDM) technique is discussed. K-band compact terminations are designed, fabricated, and measured to validate the concept. Then, the potential of this new compact topology is extended to X-band and its power handling capability (PHC) is investigated.

## II. Concept of the Topology

The topology of the termination is based on a standard free-space Salisbury screen [9]. This absorber is constituted of a resistive layer on top of a dielectric spacer. The general conditions of optimum absorption [10] lead to two conditions. The thickness of the spacer $e_s$ has to be a quarter of the wavelength $\lambda_g$ at the frequency of absorption

$$e_s = \frac{\lambda_g}{4}. \tag{1}$$

For a plane wave PW in a dielectric medium with a real part of relative permittivity $\varepsilon_r$, $\lambda_g$ is calculated by (2). For a given conductivity $\sigma$ of the resistive layer, its thickness $\tau$ is calculated by (3) so that to provide impedance equal to the one of air $Z_{0\,\mathrm{pw}}$

$$\lambda_{\mathrm{gpw}} = \frac{c}{f\sqrt{\varepsilon_r}} \tag{2}$$

$$Z_0 = \frac{1}{\sigma\,\tau} \tag{3}$$

$$Z_{0\mathrm{pw}} = \sqrt{\frac{\mu_0}{\varepsilon_0\varepsilon_r}}. \tag{4}$$

An example of topology and simulation results is given in Fig. 1. The free-space Salisbury absorber, designed to provide a strong absorption at 22 GHz, is constituted of a thin layer of tantalum nitride ($\sigma = 7400$ S/m, $\tau = 0.358$ $\mu$m) on top of a $\lambda_g/4$ spacer made of air ($\varepsilon_r = 1$) with a thickness $e_s = 3.409$ mm. Simulations were performed using Ansys HFSS[1] software with periodic boundaries. A perfect electric conductor (PEC) boundary was assigned at the bottom of the model to ensure a total reflection. As expected, this bilayer provides a strong absorption at 22 GHz with a $-15$ dB relative bandwidth (RBW) of 44.3%.

Such absorber can be adjusted to be designed in rectangular waveguide that propagate a $TE_{10}$ fundamental mode. In this

[1]Trademarked.

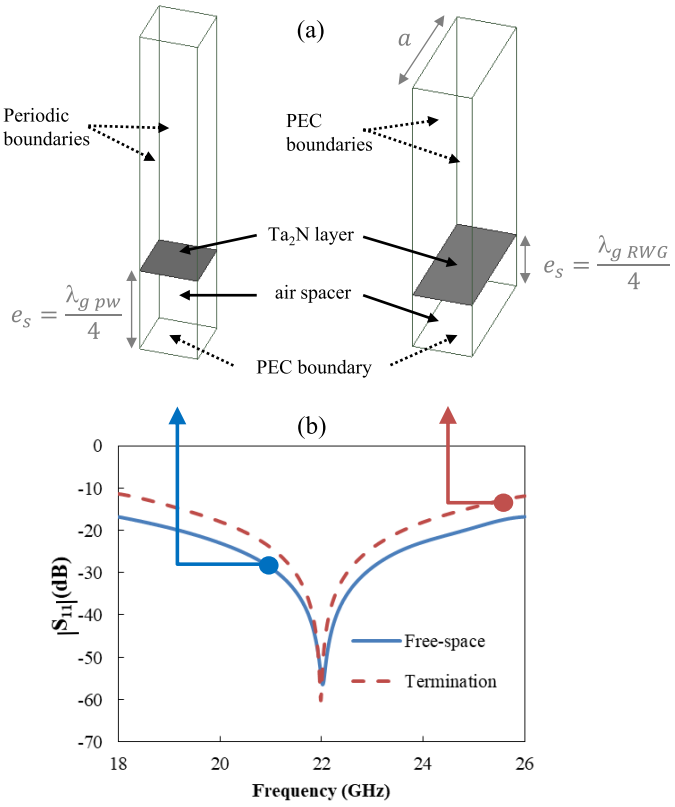


Fig. 1. (a) Simulation models of a $Ta_2N$/air Salisbury absorber in free-space (left) and rectangular waveguide (right) and (b) their reflection coefficients in K-band.

case, wavelength and impedance that have to be considered are given by the following formula:

$$\lambda_{g\,\mathrm{RWG}} = \frac{\lambda_{\mathrm{gpw}}}{\sqrt{1-\left(\frac{f_c}{f}\right)^2}} \tag{5}$$

$$f_c = \frac{c}{2a} \tag{6}$$

$$Z_{0\,\mathrm{RWG}} = \frac{Z_{0\,\mathrm{pw}}}{\sqrt{1-\left(\frac{f_c}{f}\right)^2}} \tag{7}$$

where $\lambda_{g\,\mathrm{RWG}}$ is the guided wavelength in the rectangular waveguide, $f_c$ the cutoff frequency of the $TE_{10}$ mode, $a$ the width of the waveguide, and $Z_{0\,\mathrm{RWG}}$ the impedance of this mode in the waveguide. One should note that impedance is dependent on frequency in that case.

The same materials were used to design a Salisbury absorber for a standard WR-42 K-band waveguide. Thicknesses of both air spacer and resistive layer were modified using above-mentioned equations ($\tau = 0.275$ $\mu$m, $e_s = 4.432$ mm). Fig. 1 shows that a strong absorption is achieved at 22 GHz. However, the $-15$ dB bandwidth is strongly decreased (RBW = 25.3%) compared to a free-space similar absorber due to the variation of the impedance over the frequency band under study. In Section III, we will discuss on the adaptation of the topology to be able to fabricate such component with a low-cost multi-materials 3-D printing technique.

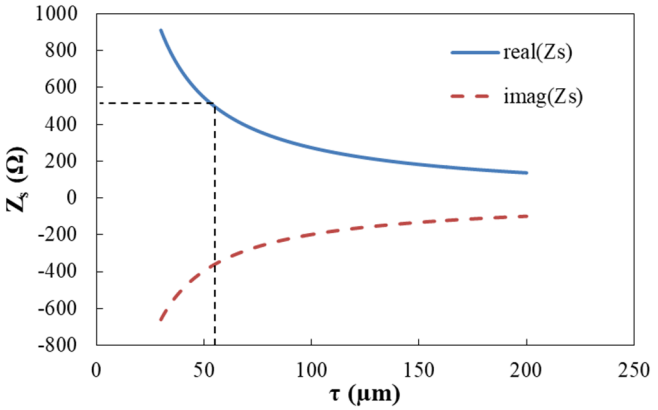


Fig. 2. Evolution of the surface impedance of a PLA-C layer as a function of the thickness layer $\tau$.

## III. Manufacturing Method and Adaptation of the Topology

### A. Multi-Materials FDM

A standard Salisbury absorber requires a low-loss dielectric and a resistive layer with a moderate conductivity that lies between 100 and 10 000 S/m to get a thickness compatible with screen-printing or deposition by sputtering or evaporation (from a few hundred of nanometers to a few tens of micrometers).

In this study, the fabrication technique is the FDM. The design of Salisbury absorber has to be adapted to take into account the manufacturing process. Especially, constraints exist on the thickness of the resistive layer. This 3-D printing technique consists in fabricating an object layer-by-layer using an extruder that pushes the material, in the form of a filament, through a nozzle that can move in a plane over a heated bed. At first, a 3-D model of the object to be printed is converted to a gcode command file using a slicing software. This file contains not only the linear movements of the printer nozzles but also the extruders and bed temperatures. The temperature-controlled extrusion head is fed with a thermoplastic material that is heated at a temperature above its fusion one. The material is deposited in layers with typical thickness of 100–200 $\mu$m and the part is built from the bottom, layer by layer. The material hardens immediately after extrusion and the bed goes down between each layer. We used a 3NTR A2v3 printer to fabricate our devices. This printer can extrude up to three different materials simultaneously.

Different FDM-compatible thermoplastics can act as low-loss dielectric. Here, we selected a polylactic acid (PLA) filament from 3-DFilTech. Its dielectric properties were extracted with a rectangular waveguide method in X-band (8–12 GHz) similar than the one used in [6]. PLA shows a permittivity of 2.67 and dielectric loss tangent of $7.5 \times 10^{-3}$ and can thus be used as a dielectric spacer in a bilayer Salisbury absorber. As the measured permittivity and loss tangent do not show a dispersive behavior in X-band so that these properties were considered for the design of the component in K-band between 18 and 26 GHz.

A carbon-filled PLA (conductive PLA from proto-pasta), called here PLA-C, was used to act as the resistive layer in the topology. Its permittivity was measured in the 1–18 GHz frequency band with a coaxial probe [11]. Measured values from [11] were extrapolated in the K-band to design the component. A permittivity that decreases from 16.1 to 14.4 between 18 and 26 GHz and loss tangent ranges from 0.78 to 0.94 in this frequency band were considered. In Section III-B, it will be shown that by slightly modifying the topology, this material can act as a resistive layer in a Salisbury absorber.

Both materials were printed with the following parameters: bed temperature = 80 °C, nozzle temperature = 200 °C, nozzle speed = 35 mm $\cdot$ s$^{-1}$.

### B. Adaptation of the Topology

As mentioned before, the dielectric spacer of the Salisbury-based rectangular waveguide termination will be constituted of a PLA layer. Equations (2), (5), and (6) lead in this case to a guided wavelength of 1.382 cm at 22 GHz in a K-band waveguide, so that the thickness of the spacer has to be $e_s$ = 2.71 mm.

In a standard Salisbury screen, the top layer is a resistive sheet whose thickness is calculated to provide impedance equal to the one in air. Here, the resistive layer will be replaced by a lossy dielectric layer made of PLA-C. In this case, the surface impedance $Z_s$ equivalent to the PLA-C layer can be calculated using the following equations where the conductivity is extracted from the measured PLA-C imaginary part of permittivity $\varepsilon''$ [12]:

$$\sigma = \omega \varepsilon_0 \varepsilon'' \tag{8}$$

$$Z_s = \frac{1}{j\omega\tau\left(\varepsilon_0(\varepsilon_r - 1) - j\frac{\sigma}{\omega}\right)}. \tag{9}$$

Fig. 2 presents the evolution of both real and imaginary parts of the surface impedance equivalent to a PLA-C layer at 22 GHz as a function of the thickness layer $\tau$. At this frequency, the impedance in a WR-42 waveguide for the $TE_{10}$ mode is equal to 490.1 Ω. This value is obtained for a thickness of 55.7 $\mu$m, a value that is very thin for FDM process and difficult to accurately achieve. Moreover, the surface impedance is complex with a negative imaginary part so that this layer will present a capacitive behavior. Finally, the thickness of this lossy layer will be not negligible compared to the total thickness of the absorber so that the propagation in this layer will contribute to the phase shift of the absorber on the contrary to a pure Salisbury screen. Thus, this bilayer can be considered as a pseudo-Salisbury absorber.

These considerations led us to consider not a full layer but fragmented layer of PLA-C layer in the form of a rectangular pad. This acts as a dilution of EM properties of the lossy layer allowing the use of thicknesses compatible with a FDM process by providing more degrees of freedom. Different shapes of PLA-C layer (cross, two pads, honeycomb) were tested in simulation but the shape does not strongly influence reflection coefficient level and bandwidth. The intermediate topology is presented in Fig. 3. The dielectric spacer is constituted of a PLA layer with a thickness $e_s$. Its transverse dimensions correspond to those of a standard WR-42 rectangular waveguide ($a$ = 10.67 mm, $b$ = 4.32 mm). The resistive

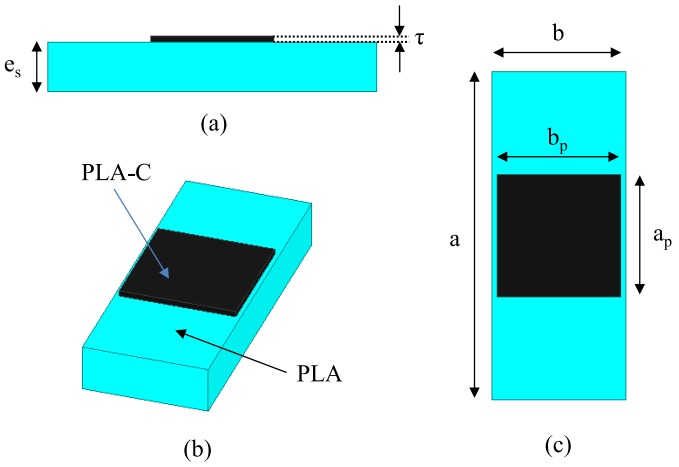


Fig. 3. (a) Side, (b) 3-D, and (c) top view of a pseudo-Salisbury absorber in rectangular waveguide.

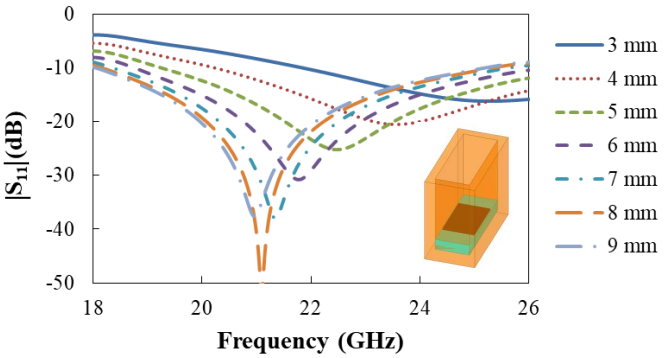


Fig. 4. Simulated reflection coefficient of a pseudo-Salisbury absorber in rectangular waveguide for different $a_p$ values ($e_s = 1.4$ mm, $b_p = 4$ mm, and $\tau = 200$ $\mu$m).

layer is replaced by a PLA-C pad with a thickness $\tau$ and whose in-plane dimensions are $a_p$ and $b_p$.

EM simulations were performed with this absorber positioned in a short-ended WR-42 waveguide for different dimensions (size and thickness of the pad, thickness of the spacer). Fig. 4 presents reflection coefficients for $e_s = 1.4$ mm, $b_p = 4$ mm, $\tau = 200$ $\mu$m, and different values of pad width $a_p$. This 1.6-mm-thick bilayer absorber can provide in simulation a strong absorption whose frequency depends on the pad dimensions. Indeed, the frequency of maximum absorption varies from 20.97 to 25.27 GHz for $a_p$ values of 9 and 3 mm, respectively. One should note that, contrary to metallic periodic surfaces, the absorption mechanism remains linked to a resonance along the direction of propagation. This figure also shows that the minimum of reflection coefficient depends on the pad dimensions. This is due to the total impedance of the bilayer that depends on the pad size and that does not match to the one of the empty waveguide for low values of $a_p$ in this case.

If the size/absorption tradeoff seems very promising, we have shown in the past that it can be difficult to confirm the performance of printed compact terminations by measurement due to dimensional uncertainties related to the fabrication and especially to the control of air gaps between the absorber and the metallic waveguide [7].

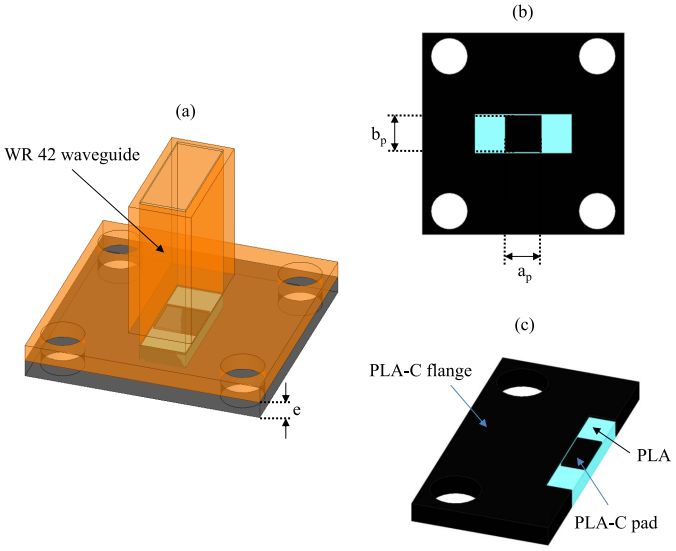


Fig. 5. Topology of the termination. (a) 3-D, (b) top, and (c) cross-sectional views (PLA in blue and PLA-C in black).

Thus, we propose to 3-D-print this bilayer pseudo-Salisbury absorber together with its own flange to get a fully flat termination that will not be affected by air gaps between the absorber and the walls of the waveguide or mispositioning. The final component is presented in Fig. 5. To avoid transversal propagation of EM wave in the flange of the termination and thus to confine it in the bilayer absorber, the flange was made of PLA-C. In simulation, a conductive boundary with a conductivity $\sigma = 2.10^6$ S/m was applied to the back face of the component to anticipate the use of a silver lacquer in practice and to ensure total reflection of the wave. Fig. 6 presents the simulated S-parameters of this component for the same dimensions $e_s$, $b_p$, and $\tau$ than the intermediate structure presented in Fig. 4. The frequency of maximum absorption $f_r$ remains strongly dependent on the pad width. For example, a 2-mm-wide pad provides a resonance frequency of 26 GHz while it moves down to 19.54 GHz for $a_p = 6$ mm. The simulated $-15$ dB RBW ranges from 15.4% to 23.1%.

One should note that the metallized PLA-C flange slightly influences the frequency of absorption. As an example, for $a_p = 4$ mm, the resonance frequency decreases from 23.56 to 22.5 GHz when a metallized PLA-C flange is considered compared to a metallic short-ended waveguide. This decrease of the resonance frequency demonstrated that PLA-C walls slightly modify the guided wavelength in the dielectric spacer section of the absorber.

In addition, vector electric field in the component is shown on Fig. 7 for a pad width $a_p = 4$ mm at the frequency of maximum absorption (22.5 GHz). This figure confirms that the absorption mechanism remains a quarter wavelength resonance of $TE_{10}$ propagation mode.

This low-weight flat termination can be directly connected to a standard waveguide. However, as the concept is based on a resonant absorber (i.e., Salisbury screen), the bandwidth of absorption will be inherently lower than traditional long wedge or pyramid that are used to fabricate wideband terminations.

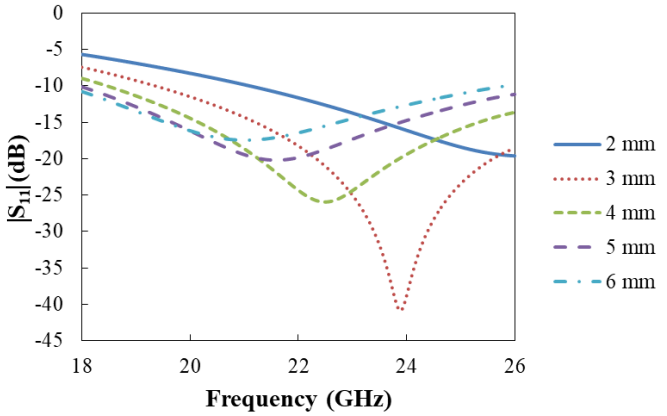


Fig. 6. Simulated reflection coefficients $S_{11}$ of the multi-material resonant termination in K-band for pad widths $a_p$ ranging from 2 to 6 mm ($e_s$ = 1.4 mm, $b_p$ = 4 mm, $\tau$ = 200 $\mu$m).

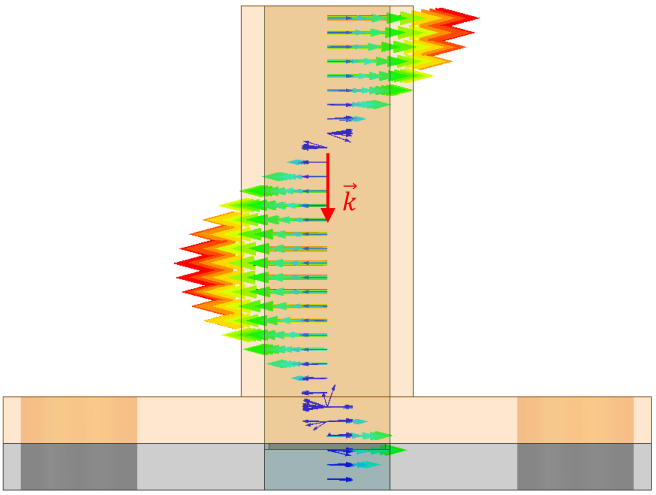


Fig. 7. Vector electric field of a multi-material termination for $a_p$ = 4 mm, $e_s$ = 1.4 mm, $b_p$ = 4 mm, and $\tau$ = 200 $\mu$m at 22.5 GHz ($\vec{k}$ represents the direction of propagation).

## IV. Fabrication and Measurements

### A. Fabrication and Reflection Measurements

Five terminations were 3-D-printed with $a_p$ ranging from 2 to 6 mm ($b_p$ = 10 mm, $e$ = 1.6 mm). Fig. 8 presents one of these devices. After fabrication, a silver lacquer was used to metallize the back face of the flange to ensure a total reflection of EM wave. The silver lacquer was cured at 60 °C during 1 h. The mass of the termination is only 0.8 g that has to be compared with the mass of a standard K-band termination which is around 40 g. Knowing that the cost of a 500 g PLA-C spool is only 78 €, the whole material cost of a termination does not exceed 0.2 €. In an industrial context, the cost would be much higher. However, manual operations would remain very limited because this component does not require post-machining except for the metallization on the back face. Considering the printing parameters, the printing time of a single component is 18 min. One should note that printing several terminations together strongly reduce the printing time par component.

A Rohde and Schwarz ZVA 67 vector network analyzer was used to measure the reflection coefficient of the terminations. A Thru-Reflect-Line calibration was first performed to put the reference plane of measurement at the output of the coaxial-to-rectangular waveguide transition. Then, terminations were screwed to the transition (see Fig. 8). For purposes of comparison, a commercial rectangular waveguide termination from Vector Telecom (VT220WL1.03PC) was also measured.

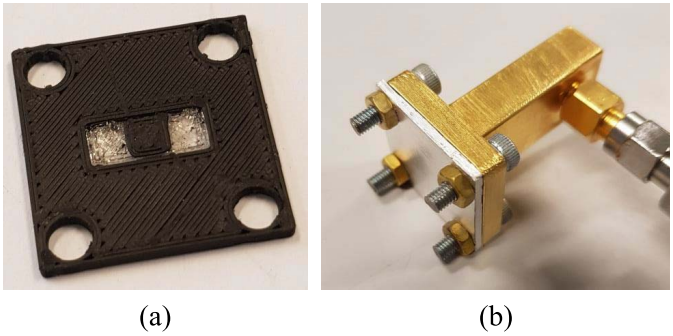


Fig. 8. Photographs of (a) K-band multi-material termination before metallization and (b) metallized termination screwed to a metallic waveguide.

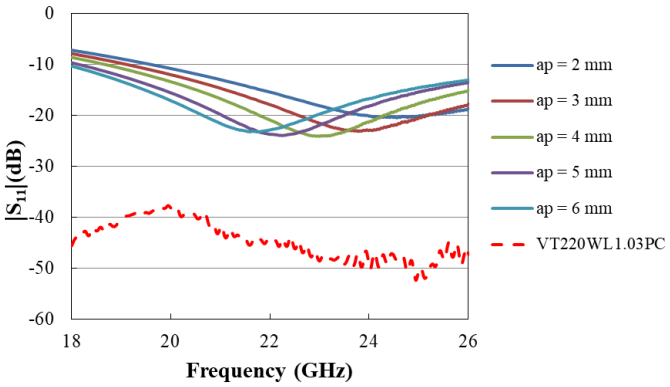


Fig. 9. Measured reflection coefficients $S_{11}$ of the multi-material resonant termination in K-band for pad widths $a_p$ ranging from 2 to 6 mm ($e$ = 1.6 mm and $b_p$ = 4 mm) compared with a commercial rectangular waveguide termination from Vector Telecom.

Fig. 9 presents the measured reflection coefficients of the terminations for different values of $a_p$. The minimum return loss at the resonance frequency is less than −20 dB for all the terminations. The −15 dB RBWs are between 17.2% and 25%. As expected, the frequency of maximum absorption is shifted toward high frequency when $a_p$ decreases. The measured frequency shift as well as the minimum return loss value as a function of $a_p$ is slightly lower than predicted by simulation. Indeed, the tuning range of absorption frequency is limited to 21.6–24.4 GHz for the $a_p$ values range under study. This reduced tuning frequency and slight disagreement between simulations and measurements could be due to wrongly estimated dielectric properties of the printed materials. Anisotropic effects linked to the path followed by the nozzle to deposit the material during the fabrication of the PLA-C pad or slight variations of dielectric properties of PLA-C along the filament spool can also affect the dielectric properties, and thus, the reflection coefficient of the termination.

As a comparison, the commercial rectangular waveguide termination provides a reflection coefficient lower than −37.7 dB over the whole K-band. This termination is more efficient and

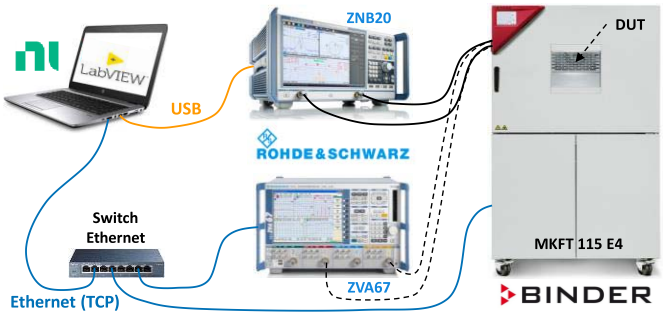


Fig. 10. Illustration of the measurement bench: materials and communication protocols used.

provide a wider bandwidth than the proposed design but its weight (40 g) and length (85 mm) are not compatible with its integration in very compact systems.

So, the proposed topology associated with multi-materials 3-D-printing allows the fabrication of low-cost low-weight ultracompact terminations dedicated to low-band low-power applications. Such printed components will not replace standard wideband termination but will provide a solution for some applications with limited band of frequencies.

### *B. Temperature Behavior*

To evaluate the temperature stability of the component, a lab-made test bench was developed (see Fig. 10). It implements specific hardware and software.

1) MKFT 115 E4 climatic chamber from Binder covering the temperature range −70 °C to +180 °C.
2) Two Rohde and Schwarz ZNB20 and ZVA67 vector network analyzers covering the frequency ranges [100 kHz; 20 GHz] and [100 MHz; 67 GHz], respectively.
3) LabVIEW 2020 software which allows controlling the whole measurement bench.
4) An Ethernet switch to establish communication between the control software and the measuring devices.

Communication between the various devices and the resulting data processing is ensured by the LabVIEW software via universal serial bus (USB) or Ethernet type buses using the transmission control protocol (TCP).

To ensure the quality of the measurements, it is necessary to make sure that the temperature is stabilized within the device under test (DUT) and not only within the climatic chamber. To do this, the program analyzes the fluctuations of the temperature in the chamber on the one hand and the S-parameters on the other. The measurement will only be done if these two data are considered to be stable.

For the temperature variations in the chamber, we follow the procedure shown in Fig. 11. Two parameters are set via the software application interface: the maximum deviation from the set temperature $T$ (0.1° by default but a lower value can be set) and the stabilization time (5 min by default) during which the temperature variations must not exceed the value $\Delta T$.

This process ensures that the temperature of the chamber is well defined but this step is not sufficient to guarantee that the temperature within the device to be characterized is also well defined. We have therefore imposed a second criterion which consists in analyzing the S-parameters. Thus, it is possible to

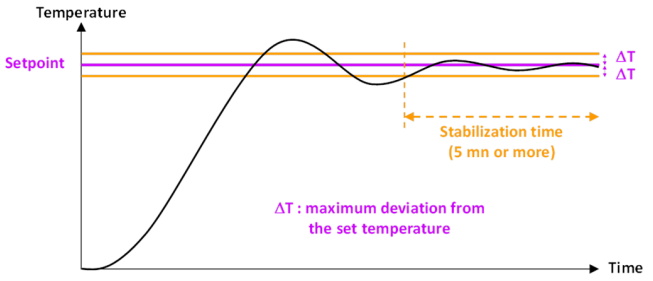


Fig. 11. Principle of temperature stabilization of the climatic chamber: the measured temperature must be equal to the set point at $\pm\Delta T$ and during a minimum stabilization period.

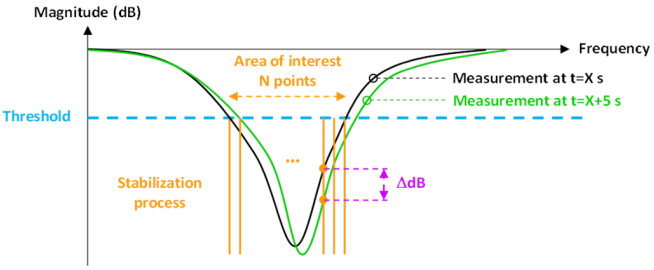


Fig. 12. Principle of stabilization of S-parameters in the case of a reflection coefficient: the difference between two consecutive measurements must be less than a limit for all frequency points in the area of interest.

work either on the reflected signal ($S_{11}$) or on the transmitted signal ($S_{21}$) depending on the DUT.

The principle is to compare the difference between two consecutive measurements separated by 5 s and to verify that this difference in magnitude is lower than a predefined limit (0.01 dB by default) for all the frequency measurement points in the area of interest (bandwidth for a filter or resonance peak for a resonator for example). The zone of interest, in which the analysis will be performed, is defined by a threshold. Fig. 12 illustrates this sequence in the case of a reflection measurement.

Temperature stabilization is only considered to be established if the two previous criteria are reached simultaneously. Once this stabilization is validated, the measurement is taken into account and saved before moving on to the next temperature point for which the temperature stabilization cycle is repeated.

This bench was used to investigate the temperature behavior of the multi-materials compact K-band termination between −20 °C and 60 °C. As an example, Fig. 13 presents S-parameters of a compact termination ($e_s$ = 1.4 mm, $a_p$ = 4 mm, $b_p$ = 4 mm, $\tau$ = 200 $\mu$m) at different temperatures. At low temperature (−20 °C), reflection coefficient tends to increase but remains lower than −20 dB in the frequency range of interest. Despite these variations, the maximum resonance frequency shift is 320 MHz and the −15 dB RBW remains between 20.8% and 25.6% in the temperature range. When considering the very compact size of the component and the related sensitivity, the temperature stability appears to be quite satisfying.

## V. Extension to Other Frequency Bands

The concept of this termination seems to be very general and we therefore tried to extend it to other frequency bands.

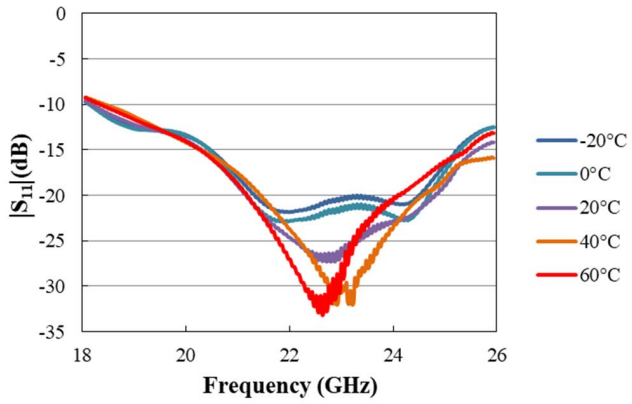


Fig. 13. S-parameters of a compact K-band multi-materials termination ($e_s$ = 1.4 mm, $a_p$ = 4 mm, $b_p$ = 4 mm, $\tau$ = 200 $\mu$m) for temperatures ranging from −20 °C to 60 °C.

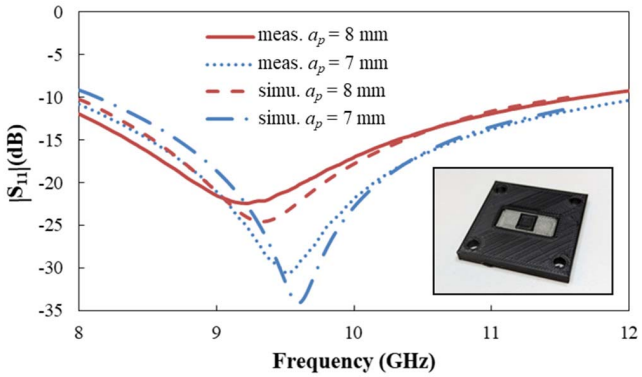


Fig. 14. Comparison between measured and simulated reflection parameters $S_{11}$ of multi-materials X-band compact terminations for $a_p$ = 7 mm and $a_p$ = 8 mm.

X-band (8–12 GHz) was chosen because we are able to evaluate the power handling of components in this frequency band.

The topology is the same than the one presented in Fig. 5 but the dimensions were adapted to be used with a standard open-ended WR-90 waveguide. As the PLA permittivity does not show any dispersive behavior, the same dielectric properties than in K-band were considered. For PLA-C whose permittivity and loss tangent strongly vary with frequency the properties given in [11] were used.

In the X-band, optimum performance was got for the following dimensions: $e_s$ = 4 mm, $b_p$ = 8 mm, $\tau$ = 400 $\mu$m. Two different terminations with $a_p$ values of 7 and 8 mm were selected. The fabrication process was the same than the one presented in Section III. The fabrication time for a single component is around 1 h and the material cost is evaluated to about 1.2 €.

Simulated and measured reflection coefficients for both $a_p$ values are presented in Fig. 14 and their characteristics compared in Table I.

As in K-band, the frequency of maximum absorption can be controlled by the size of the pad. The agreement between simulation and measurement is satisfying with a maximum deviation of 110 MHz (1.1%) on the center frequency. The RBW

TABLE I

COMPARISON OF CENTER FREQUENCY AND RBW OF X-BAND MULTI-MATERIALS TERMINATIONS

| | Simulation | | Measurement | |
|---|---|---|---|---|
| $a_p$ (mm) | 7 | 8 | 7 | 8 |
| $f_r$ (GHz) | 9.715 | 9.445 | 9.635 | 9.335 |
| RBW (%) | 20.5 | 19.2 | 23.1 | 20.9 |

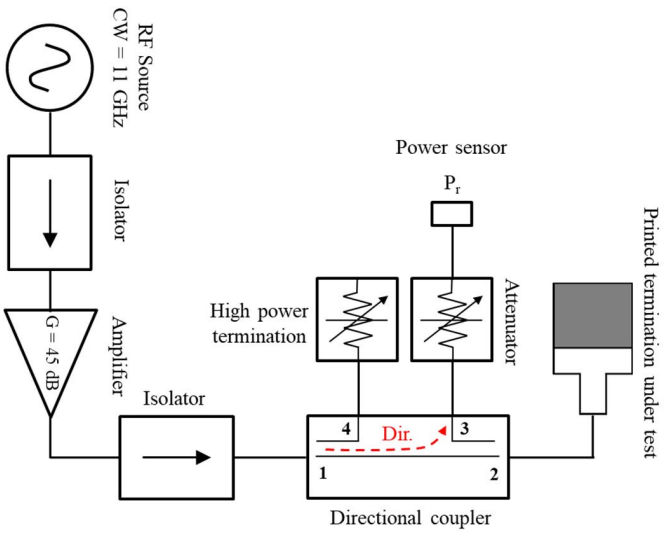


Fig. 15. Schematic of the power test bench.

is very similar to that obtained on K-band terminations with a value around 20%. These measurements demonstrate that this multi-material topology is a very flexible concept that can be applied to a wide range of frequencies, and therefore, to associated applications.

## VI. POWER HANDLING CAPABILITY

The PHC of FDM-based components is lower than that of ceramic component limiting their use to low-power applications. To identify the potential applications of these components, the evaluation of the PHC has been performed with the power test bench presented in Fig. 15. The main components of the bench are: an Agilent 8757E scalar network analyzer used as a continuous wave (CW) source, a AA-MCS 30 W 6–12 GHz power amplifier, a HP 772D 2–18 GHz directional coupler, and a R and S NRP67T power sensor. The measurement frequency of 11 GHz was chosen so that the directivity of the coupler was minimum to ensure a difference of more than 30 dB between the leakage of incident signal and the signal reflected by the termination. The incident power level was first calibrated by positioning the power sensor in place of the component under test.

A standard wedge termination was designed and 3-D printed (only with PLA-C) to compare its PHC to the one of the multi-materials' compact termination. To ensure the same reflection coefficient than the compact termination at 11 GHz, the length of the wedge termination has to be 21 mm, i.e.,

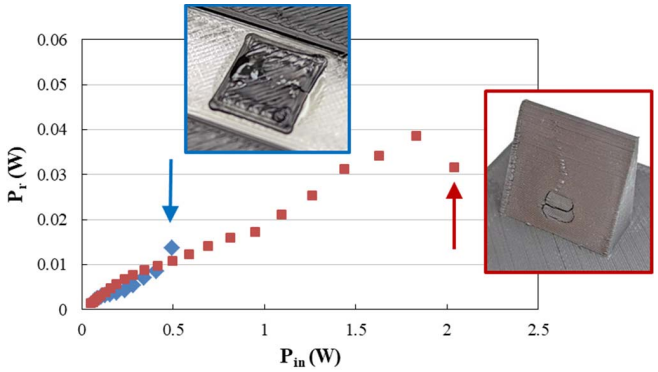


Fig. 16. Evolution of the reflected power as a function of the incident power at 11 GHz for standard wedge and compact multi-materials terminations. Inset: Heat damaged standard wedge (red line) and compact multi-materials (blue line) terminations. The arrows indicate the assumed start of the component degradation.

a size approximately 5 times higher than the compact one. The procedure was the following.

1) A first measurement of the reflected power $P_r$ is performed at a low incident power level ($P_{\text{in}} = 0.07$ W).
2) The incident power level is increased and the reflected power is measured when stabilization is reached.
3) The incident power is decreased to the minimum level and the reflected power is compared to the initial measurement so that to ensure that the critical incident power is not reached and that an irreversible damage does not occur.

This procedure is continued until a significant change ($\pm 1$ dB) in the reflected power at low incident power level is observed.

Fig. 16 shows the evolution of the reflected power $P_r$ as a function of the incident power $P_{\text{in}}$ for the two terminations. The compact termination presents a quite linear evolution up to 0.49 W. For higher power values, the slope, which is directly related to the reflection coefficient of the component, increases sharply. We suppose that the change of slope is due to a change in the behavior of the material, most probably passing from a glassy state to a rubbery state in a sufficient way for the phenomenon to be irreversible. It is worth noting that this is an amorphous thermoplastic matrix composite. It is difficult to identify the actual beginning of the damage of the component because there is not a drastic change in the reflection coefficient of the termination. However, after this measurement, a fusion zone is visible on the PLA-C pad.

For the wedge termination, the reflected power as a function of incident power remains quite linear up to 2.04 W. The oscillation at lower power levels may be related to temperature-dependent changes in EM properties and/or material expansion. A large, damaged zone can be seen at the base of the wedge after this measurement.

One should note that these experiments were done on two different samples of each termination type and provided similar results. To go further in the evaluation of this PHC, multiphysics simulations were performed. Ansys HFSS[1] software is used to perform an EM simulation.

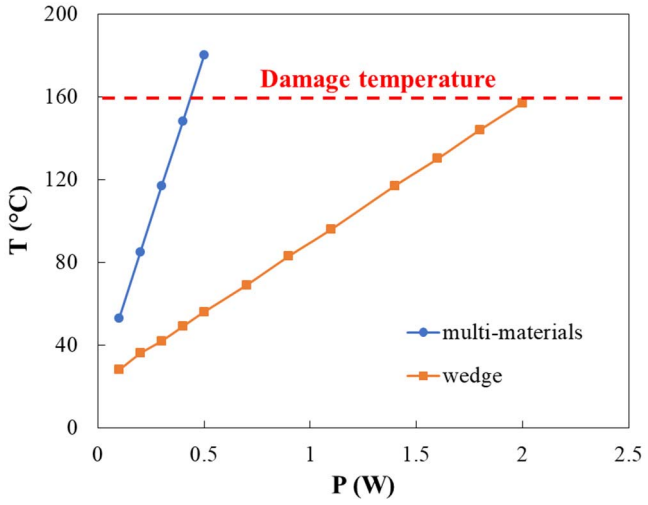


Fig. 17. Simulated evolution of the maximum temperature as a function of incident power for standard wedge and multi-materials compact terminations at 11 GHz.

As a first approximation, the intrinsic characteristics of the printed materials (permittivity, loss tangent) are assumed to be independent of temperature. The Ansys Workbench[1] software, allows making a direct link between the EM simulation and the thermal simulation performed under Mechanical[1] software.

In these simulations, the isotropic thermal conductivity of the considered materials is 0.144 W $\cdot$ m$^{-1}\cdot$°C$^{-1}$ for PLA and 400 W $\cdot$ m$^{-1}\cdot$°C$^{-1}$ for copper, respectively. The heat transfer coefficient of the air is 10 W $\cdot$ m$^{-2}\cdot$°C$^{-1}$ and the initial temperature is 22 °C.

The temperature evolution in the component has been studied for each topology in the 0.1–2 W power range. Fig. 17 shows the evolution of the maximum temperature in both components as a function of the incident power (CW at 11 GHz). The fusion temperature of PLA is 160 °C. It is observed that the irreversible temperature is achieved for a critical incident power of 0.44 and 2 W for the compact multi-materials termination and wedge termination, respectively. These simulation results are in good agreement with the measured behavior observed on Fig. 16.

Fig. 18 shows the thermal mapping at 11 GHz at critical maximum incident power levels for both terminations under study. It highlights the influence of the shape on the heat distribution, and thus, on the PHC of the components.

These experimental and simulated evaluations of the PHCs seem to demonstrate that the compact multi-materials termination maximum power handling is more than four times lower than the one of the standard topology. This is due to a worse distribution of heat which results in a higher concentration of heat at critical point.

Even though simulations and experiments are in quite good agreement, further investigations have to be performed. At first, it is difficult to identify the beginning of the damage for such rectangular waveguide terminations. Performing measurements on open structures, such as planar terminations, would allow a better identification of the onset of fusion. Then, default values (workbench libraries) are currently used to perform multiphysics simulations and the same thermal

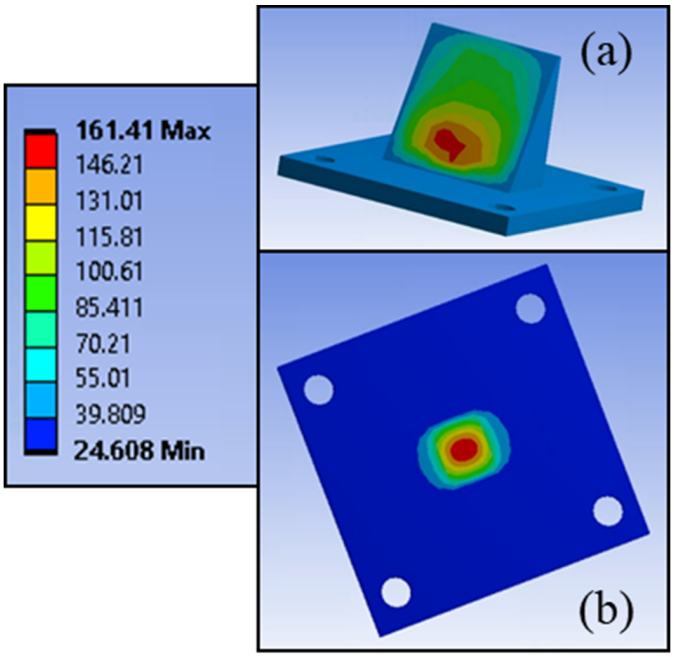


Fig. 18. Thermal mapping for (a) standard wedge termination made of PLA-C for an incident power $P_{\text{in}} = 2$ W and (b) compact multi-materials termination for an incident power $P_{\text{in}} = 0.44$ W at 11 GHz.

properties are used for PLA and PLA-C materials. Additional measurements will be soon performed to better evaluate thermal conductivities, coefficients of thermal expansion, specific heat values, and temperature dependence of dielectric properties. One should note that PHC can be drastically improved using materials with higher fusion temperatures and/or higher thermal conductivities such as polyphenylene sulfide (PPS)-, polyetherketoneketone (PEKK)- or polyetheretherketone (PEEK)-based filaments [13], [14].

## VII. Discussion

Table II compares performance of our terminations with literature. This table indicates the RBW together with the length of the components divided by the wavelength at the center frequency $\lambda_0$ and their volume divided by the cube of the wavelength at the center frequency $\lambda_0^3$ so that to calculate normalized length and volume independent on frequency band. The normalized volume will make it possible to compare the compactness of the different terminations.

The shortest termination is achieved in [1] with a length of 0.03 $\lambda_0$. However, this length corresponds to the PCB thickness that has to be integrated in a short-ended metallic waveguide. Moreover, the −15 dB RBW of this component is drastically low.

Terminations developed in [3] and [4] present high RBW but cannot be considered as compact as their length are several times longer than wavelength at their center frequency.

The most interesting components are developed in [2]. The length of the functional part, i.e., PCB power dividers, is only 0.07 $\lambda_0$ to 0.09 $\lambda_0$ and their RBW are between 14.2% and 27.3%. However, these planar power dividers require a dedicated metal housing to integrate 50-Ω resistors so that the effective volume of these components were estimated to be 1.6 $\lambda_0^3$.

TABLE II
Comparison of Performance With Literature

| Ref. | Freq. | RBW (%) | Length/$\lambda_0$ | Vol./$\lambda_0^3$ * |
|---|---|---|---|---|
| [1] | X | 0.6 | 0.03 | - |
| [2] | X | 14.2 | 0.07 # | 1.6 |
| [2] | X | 27.3 | 0.09 # | 1.6 |
| [3] | Ka | 38.7 | 3.13 # | 1.5 |
| [4] | Ka | 40.6 | 5.30 | 5.9 |
| This work (WT@) | X | 15.4 | 0.66 | 1.1 |
| This work (MMT&) | X | 23.1 | 0.13 | 0.2 |
| This work (MMT&) | K | 25 | 0.12 | 0.3 |

# Length of the functional part of the component without metal housing divided by the wavelength at the center frequency
* Estimation of the total volume of the component divided by the cube of the wavelength at the center frequency
@ WT: wedge termination
& MMT: multi-materials termination

Our components have a maximum length of 0.13 $\lambda_0$, two times higher than components in [2]. However, as flanges are printed together with the functional part of the termination (i.e., Salisbury resonator), the total length is not greater than the length of the resonator. The total volume of these standalone multi-materials terminations is less than 0.3 $\lambda_0^3$, thus 5 times lower than other published terminations. This demonstrates that this new concept can lead to efficient ultracompact terminations that can be easily integrated in different architectures.

## VIII. Conclusion

A compact multi-materials topology of rectangular waveguide terminations is proposed. This topology, based on a Salisbury resonant absorber, can be fabricated by multi-materials 3-D printing in a single process so that very low-cost low-weight components can be produced. The concept has been experimentally validated in K-band (18–26 GHz) and X-band (8–12 GHz) thus demonstrating the flexibility of the topology and fabrication process. For the moment, the PHC of the component limits the applications to low-power systems with moderate RBW (around 20%).

Further improvements can be done. To increase the bandwidth, a superposition of PLA-C/PLA bilayers can be considered in an approach similar to Jaumann absorbers in freespace. Moreover, we are planning to study other printable polymers and composites with higher fusion temperatures and thermal conductivities that could improve the behavior of the terminations in harsh environment and/or higher power systems.

## References

[1] J. Li, F. Wang, G. Wen, Y. Huang, and W. Zhu, "Planar metamaterial for matched waveguide termination," *Appl. Comput. Electromagn. Soc. J.*, vol. 28, no. 12, pp. 1236–1242, Dec. 2013.

[2] L. Guo, J. Li, H. Shao, and K. Song, "Design of rectangular waveguide to microstrip power dividers and their application as compact rectangular matching terminations," in *Proc. IEEE Asia–Pacific Microw. Conf. (APMC)*, Singapore, Dec. 2019, pp. 464–466.

[3] C. Tang, X. Pan, F. Cheng, and X. Lin, "A broadband microstrip-to-waveguide end-wall probe transition and its application in waveguide termination," *Prog. Electromagn. Res. Lett.*, vol. 89, pp. 99–104, 2020.
[4] M. Shu, C. Guo, X. Shang, W. Zhu, and A. Zhang, "A $Ka$-band wideband matched load based on lossy waveguide structures," *IEEE Microw. Wireless Compon. Lett.*, vol. 30, no. 11, pp. 1045–1048, Nov. 2020.
[5] Y. Arbaoui, V. Laur, A. Maalouf, and P. Queffelec, "3D printing for microwave: Materials characterization and application in the field of absorbers," in *IEEE MTT-S Int. Microw. Symp. Dig.*, Phoenix, AZ, USA, May 2015, pp. 1–3.
[6] Y. Arbaoui *et al.*, "Full 3-D printed microwave termination: A simple and low-cost solution," *IEEE Trans. Microw. Theory Techn.*, vol. 64, no. 1, pp. 271–278, Jan. 2016, doi: 10.1109/TMTT.2015.2504477.
[7] A. Pen, A. Chevalier, A. Maalouf, and V. Laur, "X-band compact microwave terminations," in *Proc. Asia–Pacific Microw. Conf. (APMC)*, Kyoto, Japan, Nov. 2018, pp. 315–317.
[8] V. Laur, A. Maalouf, A. Chevalier, P. Laurent, and G. Zinkiewicz, "Ultra-compact K-band microwave terminations," in *Proc. IEEE Radio Wireless Symp. (RWS)*, Las Vegas, NV, USA, Jan. 2022, pp. 1–4.
[9] R. L. Fante and M. T. McCormack, "Reflection properties of the Salisbury screen," *IEEE Trans. Antennas Propag.*, vol. AP-36, no. 10, pp. 1443–1454, Oct. 1988.
[10] B. Chambers, "Optimum design of a Salisbury screen radar absorber," *Electron. Lett.*, vol. 30, no. 16, pp. 1353–1354, Aug. 1994.
[11] V. Laur, A. Maalouf, A. Chevalier, and F. Comblet, "Three-dimensional printing of honeycomb microwave absorbers: Feasibility and innovative multiscale topologies," *IEEE Trans. Electromagn. Compat.*, vol. 63, no. 2, pp. 390–397, Apr. 2021.
[12] F. Costa, A. Monorchio, and G. Manara, "Analysis and design of ultra thin electromagnetic absorbers comprising resistively loaded high impedance surfaces," *IEEE Trans. Antennas Propag.*, vol. 58, no. 5, pp. 1551–1558, May 2010.
[13] L. Martinez *et al.*, "Development of a high temperature printable composite for microwave absorption applications," *AIMS Mater. Sci.*, vol. 8, no. 5, pp. 739–747, Dec. 2021.
[14] V. Laur, M. K. Abboud, A. Maalouf, D. Palessonga, A. Chevalier, and J. Ville, "Heat-resistant 3D printed microwave devices," in *Proc. IEEE Asia–Pacific Microw. Conf.*, Kyoto, Japan, Nov. 2018, pp. 1318–1320.

**Gautier Zinkiewicz** was born in Brest, France, in 2000. In 2021, he finished a two-year course in electronics engineering (DUT GEII) at the Technical College (IUT), Brest. He then completed a ten-week internship with the Lab-STICC Laboratory, Brest.

He focused on the automation of a test stand for microwave measurements of components and materials. He is currently an Apprentice Engineer of electronics with INSA Rennes, Rennes, France. His apprenticeship company is DGA, Bruz, France. He focuses in the electronic warfare area.

**Alexis Chevalier** received the Ph.D. degree in electronics from the University of Bretagne Occidentale, Brest, France, in 1998, for his contributions in characterization and modelization of microwave propagation in composites materials.

He acted as a Telecom Engineer with Alcatel enterprise for some years and then he joined the University of Brest, Brest, in 2003. He is currently an Associate Professor with the Lab-STICC Laboratory, Brest. His research activities focus on electromagnetic (EM) properties of materials for microwave engineering. He focuses on developing new measurements methods and models to characterize and predict microwave properties of heterogeneous, anisotropic, absorbing, dielectric, or magnetic materials.

**Paul Laurent** received the Ph.D. degree in electronics from the University of Brest, Brest, France, in 1994.

Since 1997, he has been an Assistant Professor with the Electronic Department, Technology University Institute, Université de Bretagne Occidentale (UBO), Brest. He is currently conducting research with the Lab-STICC Laboratory, Brest. He has studied different planar tunable microwave devices using liquid crystal (phase shifters, antennas, filters, etc.). He focuses on frequency agility potential are extended to the use of ferromagnetic composite or ferroelectric thin films. His current research interests include tunable microwave and RF systems.

**J. Benedicto** (Member, IEEE) received the Ph.D. degree in physics from the University of Blaise Pascal, Clermont-Ferrand, France, in 2013.

During her Ph.D., she investigated the potential of metallo-dielectric multilayers, flat lenses with subwavelength resolution, and nonlocality in metals. In 2013, she held a post-doctoral position with the Fresnel Institute, Marseille, France. The fields of application of her post-doctoral research were hybrid magnetic-electric dielectric scatterer near-field and far-field analyses. In 2015, she became an Assistant Professor with the Lab-STICC, Brest, France. Her current research interests include the approach and optimization of microwave breakdown phenomena (multipactor), and the multiphysics modeling of RF materials and devices.

**Azar Maalouf** received the Ph.D. degree in physics from the University of Rennes 1, Rennes, France, in 2007.

In 2011, he became a Research Engineer at the Lab-STICC, Brest, France. His main scientific interests include the physical chemistry of materials and particularly the study and the implementation of these materials in thin, thick, or massive layers. The fields of application are rechargeable batteries and accumulators from 2001 to 2003, study and fabrication of optical waveguides and optical communications from 2003 to 2010, and the study and fabrication of circuits operating in the microwave domain since 2011.

**Vincent Laur** (Senior Member, IEEE), received the Ph.D. degree in electronics and the Habilitation à Diriger des Recherches [accreditation to supervise research] degree from the University of Brest, Brest, France, in 2007 and 2019, respectively.

In 2008, he was a Post-Doctoral Fellow with the XLIM Laboratory, Limoges, France. He is currently a Full Professor and the Head of the Smart Materials and Related Technology Team, Lab-STICC Laboratory, Brest. He has authored or coauthored more than 120 papers in international peer-reviewed journals and conference proceedings. His current research interests include the characterization, modeling, and integration of functional materials (ferroelectrics, ferromagnetics, ferrites, etc.) for microwave applications. He focuses on the application of new technologies (3-D printing, 3-D metallization, molded interconnect devices, nanomaterials, etc.) in the microwave domain.

Dr. Laur frequently acts as a reviewer for several technical publications.